Digital Beam Forming Concepts with Application to Spaceborne Reflector SAR Systems

Sigurd Huber, Marwan Younis, Anton Patyuchenko and Gerhard Krieger
Microwaves and Radar Institute, German Aerospace Center (DLR)
Muenchner Str. 20, 82234 Wessling, Germany
sigurd.huber@dlr.de

***Abstract*—The trend in the conception of future spaceborne radar remote sensing is towards the use of Digital Beam Forming (DBF) techniques. These systems will comprise multiple digital channels, where the analog-to-digital converter is moved closer to the antenna. This dispenses the need for analog beam steering and by this the use of transmit/receive modules for phase and amplitude control. Digital beam forming will enable Synthetic Aperture Radar (SAR) which overcomes the coverage and resolution limitations applicable to state-of-the-art systems. Moreover, new antenna architectures, such as reflectors, already implemented in communication satellites, are being reconsidered for SAR applications. This paper is dedicated to the digital signal processing aspects of such reflector based SAR systems. After introducing the hardware concepts the beam forming algorithms are presented and demonstrated by means of numerical simulations.**

I. Introduction

Synthetic aperture radar, utilizing digital beam forming, is increasingly being considered for future earth observation missions. This is evident both from research activities [1], [2] and space qualified technology demonstrations [3]. One of the reasons for this trend is that state-of-the-art SAR systems can not fulfill the heterogeneous demand on products at the required performance level. The motivation for using digital beam forming techniques is their ability to provide simultaneously a wide swath and a high resolution. In this paper DBF concepts for reflector based SAR systems are presented with the main objective to improve the Signal to Noise Ratio (SNR). Aside from this, the impact of pointing errors on the interferometric phase is investigated. In the last section a peculiarity of reflector systems with feed arrays, which is the frequency dependence of the antenna pattern, is presented and adequate signal processing concepts are proposed.

II. Reflector System Architecture

The reflector system consists of a parabolic reflector and a feed array of transmit/receive elements, as shown in Figure 1. The feed elements are arranged in the plane perpendicular to the flight direction and facing the reflector. Each element results in a beam, illuminating a region on the ground, which partially overlaps with the region illuminated by the beams of the adjacent elements. To illuminate a given angular segment in elevation, the corresponding feed elements are activated. Depending on the scan angle, one or more elements need to be activated, to avoid SNR loss. The receive beam will scan the complete swath within the time period of one PRI, whereas each element is only active during a subinterval of this time period. On transmit all N elements are activated generating a wide beam.

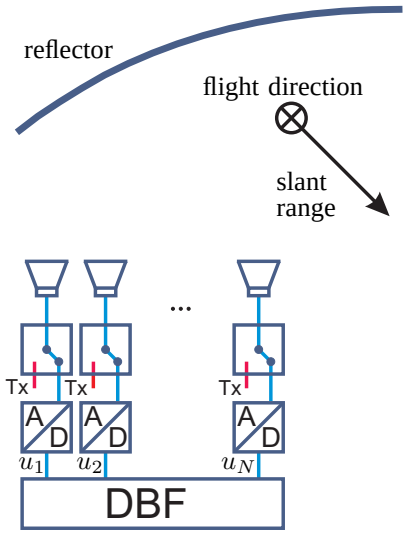

Fig. 1. System architecture for reflector system; some components such as LNAs, T/R-modules, mixers, filters etc. are not shown to maintain a clear representation.

III. Digital Beam Forming Concepts

Generally the digital beam-forming concepts, considered in this paper, aim at an improvement of the system performance, namely the SNR, the robustness of the interferometric phase against pointing errors as well as signal modulation effects induced by the frequency dependent antenna pattern.
The input to the digital beam former is a N-dimensional raw data vector $\mathbf{u}(t) = [u_1 u_2 ... u_N]^\top(t)$ as indicated in Figure 1. This signal is modeled as the received waveform $s(t)$ weighted with the individual complex channel pattern $\mathbf{g}(\theta) = [g_1 g_2 ... g_N]^\top(\theta)$ and superimposed by thermal receiver noise $\mathbf{n}(t) = [n_1 n_2 ... n_N]^\top(t)$ of power proportional to the receiver bandwidth.

$$\mathbf{u}(t) = \mathbf{g}(\theta)s(t) + \mathbf{n}(t) \quad . \tag{1}$$

The sampled beam-former output is a weighted linear combination of the input raw data signals

$$u_{\mathrm{DBF}}(k) = \mathbf{w}^\top(k)\mathbf{u}(k) \quad . \tag{2}$$

Assuming mutually independent signal and noise channels, the beam former output SNR can be written as

$$SNR(k) = \frac{\sigma_s^2}{\sigma_n^2} \frac{|\sum_i w_i g_i|^2}{\sum_i |w_i|^2} \quad . \tag{3}$$

Based upon equation (2) different digital beam-forming techniques are introduced in the next subsections.

A. Digital Beam Forming in Elevation

Digital beam forming in elevation denotes an operational mode, generating a wide transmit beam that illuminates the complete swath and a narrow, high gain beam on receive that follows the pulse echo on ground. Adverse to planar phased array antennas, in the reflector case a single activated feed element allows to illuminate only a small solid angle. This means that adjacent feed element patterns do not overlap substantially. The consequence is that during the scan process different receive channels have to be switched on or off. The number of activated elements at a given time instance is dictated by the duration of the pulse and the beam widths of the single channel pattern. Looking at a certain direction

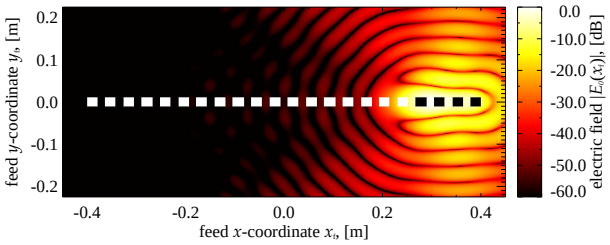

Fig. 2. Normalized electric field on the feed array due to an extended pulse on the swath edge.

θ, the corresponding channel has to be open until the signal completely has entered the system. Since the echo on ground moves on, additional receive elements have to be switched on. Figure 2 shows the field strength distribution on the feed plane due to an extended pulse in near range. The field is concentrated over a subset of feed elements, where the activated elements are represented by black patches.
In the notation of equation (2) the corresponding weight vector would look like this:

$$\mathbf{w}(k) = [0...01111]^\top \quad , \tag{4}$$

where 1 denotes an activated feed element and 0 indicates a switched off channel. Inserting equation (4) into (3) yields

$$SNR(k) = \frac{\sigma_s^2}{\sigma_n^2} \frac{1}{N_{\mathrm{act}}} \left| \sum_{i=m}^{m+N_{\mathrm{act}}-1} g_i \right|^2 \quad . \tag{5}$$

By this rudimentary beam forming method it becomes clear, that the receive gain will drop proportional to the number of activated elements N_{act}.

B. Conjugate Field Matching

To overcome the large gain loss, a time varying weighting method, based on the Conjugate Field Matching (CFM) [4] principle can be applied. By this method the individual channel weights are chosen as the conjugate complex of the incident field on the feed elements.

$$\mathbf{w}(k) = \mathbf{g}^*(k) \quad . \tag{6}$$

In analogy to (5) the corresponding SNR is found to be

$$SNR(k) = \frac{\sigma_s^2}{\sigma_n^2} \sum_{i=m}^{m+N_{\mathrm{act}}-1} |g_i|^2 \quad . \tag{7}$$

In principle CFM allows to activate all N channels on receive simultaneously. Those channels contributing predominantly with noise are quasi nulled with small magnitude weights. Since the signals are also combined according to their phase, the high receive gain can be reconstructed at every time instance.

C. Frequency Adaptive Filtering

The afore mentioned principles are adequate for short pulse lengths. Consider the baseband raw data signal u_i in Figure 3(a) originating from two point scatterers. The selected waveform is a chirp, common for spaceborne SAR systems. Since both scatterers are observed under different aspect angles, they are also weighted with different feed element patterns. Consequently the weight w_i chosen for example for $k = 1000$

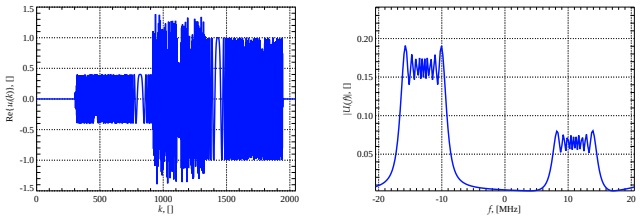

(a) raw data (b) spectral domain

Fig. 3. Raw data signal u_i for two point scatterers for a single channel (left); Fourier spectrum of the raw data stream sequence for $k \in [1000, 1200]$ (right)

can only match the one signal or the other. The solution to this problem is the use of a frequency adaptive filter. Taking the Fourier transform of the overlap region between $k = 1000$ and $k = 1200$ results in two separated spectra. In Figure 3(b) the low frequency part of the large amplitude signal can be clearly distinguished from the high frequency part of the low amplitude signal. Each spectral part can now be weighted individually by means of CFM. The filter can be implemented as a Finite Impulse Response (FIR) filter, as shown for the ith channel in Figure 4. $J + 1$ is the total number of time variant filter coefficients $w_{i,j}(k)$ per channel and the filter order is J. This digital beam-forming approach overcomes the limitations from temporally extended pulses.

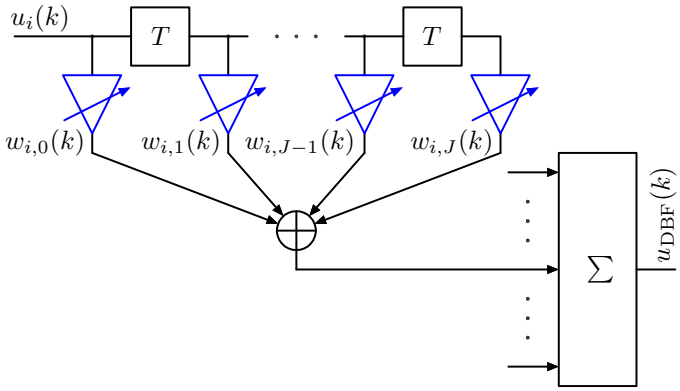

Fig. 4. FIR filter with time variant coefficients.

D. Simulations

In the following, simulation results for four different digital beam forming algorithms are presented.

- CFM after RC: The first algorithm serves as a reference, since it is independent from the pulse length and therefore performs optimal. The basic idea is to range compress the individual channel raw data streams prior to beam forming. The raw data signals of the activated channels N_{act} are than combined utilizing CFM according to equation (6). The draw back is clearly the high standard of the digital beam former hardware, where digital filters with thousands of coefficients would be required.
- f-adaptive: The second algorithm is the frequency adaptive beam former. Obviously the hardware requirements are relaxed, since FIR filters with only 31 time variant coefficients for this simulation configuration are necessary.
- ”1”: The third method is the basic unity weighting beam former according to (4).
- CFM: The forth beam former uses CFM weights (6) without any further processing.

Figure 5 shows a realization of the relative SNR over ground range. Clearly the frequency adaptive beam former (blue

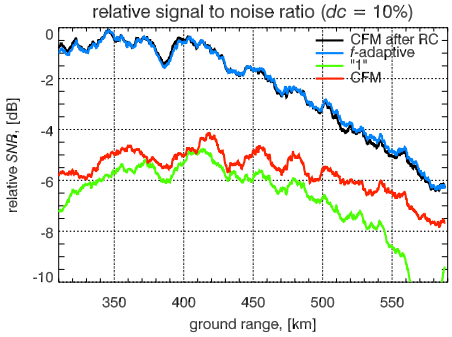

Fig. 5. Relative SNR for a duty cycle of $10\,\%$ corresponding to a pulse length of $62\,\mu$s.

curve) performs as good as the CFM based algorithm after range compression (black curve) with a drastically reduced hardware effort. CFM without further processing (red curve) suffers from weight mismatch especially in near range and the conventional channel combination approach (green curve) yields a SNR degradation proportional to the number of activated channels N_{act} as predicted by equation (5).

Important for interferometric applications is the behavior of the interferometric phase in the presence of pointing errors. Figure 6 shows the interferometric phase error for a mispointing $\Delta\theta$ of $0.1°$. In this simulation thermal receiver noise is not considered in order to visualize the effects only resulting from the antenna. For a clear representation the individual curves have been displaced in the vertical direction. The

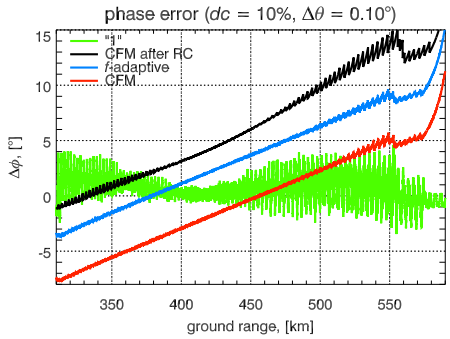

Fig. 6. Mispointing induced interferometric phase error simulation without thermal receiver noise.

CFM based DBF approaches result in an approximately linear phase ramp, which can be calibrated to a certain degree. The unity weighting algorithm produces periodic phase jumps, due to phase discontinuities in the channel phase patterns. These interferometric phase errors are difficult to impossible to calibrate.

1) Modulation Effects: Two common reflector system configurations are the offset- and the center-fed-configuration. In the offset case the feed array is moved out of the focal point or even out of the focal plane. This grants minimal interference between the primary field produced by the current distribution on the reflector and the feed array. The disadvantage of out-of-focus configurations is a broadening of the pattern as well as a gain loss. Depending on the transmitted wavelength, center fed reflector systems can suffer severely from multipath effects between the reflector and the feed system. In [5] it was shown that the blockage of the feed array introduces a frequency dependence of the antenna gain pattern. In Figure 7(a) an example of the Tx gain pattern as function of the elevation scan angle θ for a center fed L-band system for three frequencies is presented. This gain variation modulates the signal as indicated by the point target spectrum in Figure 7(b) for scan angle $\theta = 0°$. It is important to note that the modulation due to the transmit- and receive-pattern has to be taken into account. This modulation will result in an unwanted degradation of the SAR impulse response function.

In the following two strategies to deal with this problem shall be outlined. If the goal is to optimize the SNR, the usual

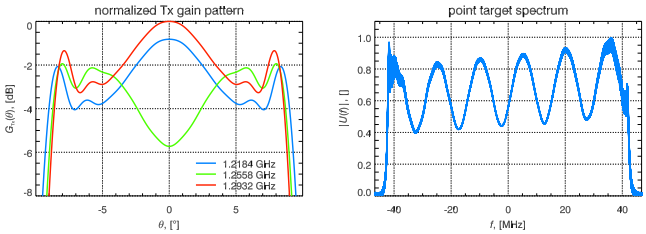

(a) Tx gain pattern (b) modulated spectrum

Fig. 7. Blockage induced frequency modulation of the gain pattern (left) and effect on the received signal (right).

approach involves the use of a matched filter. In this case the space-time adaptive filter coefficients also become frequency dependent and equation (6) is modified according to

$$\mathbf{w}(k,f) = \mathbf{g}^*(k,f) \quad . \tag{8}$$

The resulting output signal after the beam former is presented in Figure 8(a). As expected the matched filter approach results in a accentuation of the modulation. If this modulation is not compensated in the SAR range processing, the resulting impulse response will be distorted.

Another strategy is to preserve the rectangular envelope of the waveform at the cost of a slight loss of SNR. This could be done by applying the inverse of the pattern to the filter coefficients. The drawback is that pattern nulls will produce singularities in the filter coefficients and hence cause filter instability. The method exploited here is to normalize the filter coefficients to the maximum of the frequency dependent pattern for each frequency. The ith channel time and frequency dependent coefficient then takes the from

$$w_i(k,f) = \frac{g_i^*(k,f)}{\max\left\{|g_i(k,f)|^2\right\}} \quad . \tag{9}$$

Figure 8(b) shows the beam former output using coefficients (9). In Table I the range compressed beam former output using

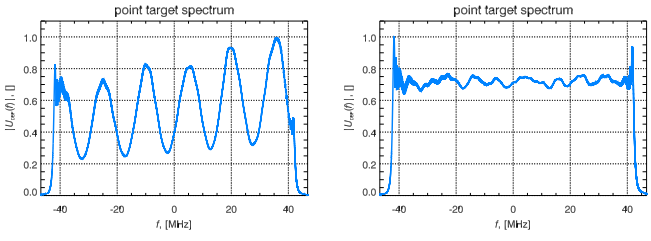

(a) matched filter spectrum (b) compensated spectrum

Fig. 8. Point target spectra using a matched filter (left) and applying compensation (right).

the matched filter (8) approach and the compensated matched filter (9) method is compared to a reference case (ref.) where an ideal chirp signal is filtered. Though the peak side lobe ratio ($PSLR$) and the slant range resolution (Δr) is in the same order for all three cases, the integrated side lobe ratio ($ISLR$) for weights (8) is about a factor of two larger. It shows when looking at the impulse response, that a lot of signal energy is concentrated in two large side lobes.

It is important to mention, that the number of filter coefficients had to be increased from 31 to 91 in order to adapt to the envelope of the spectrum. Also the computation of the complex weights becomes more involved, since now also the transmit pattern has to be taken into account compared to frequency independent antenna pattern.

TABLE I
IMPULSE RESPONSE PARAMETERS FOR THE TWO BEAM FORMERS AND A REFERENCE CASE

	$PSLR$, [dB]	$ISLR$, [dB]	Δr, [m]
ref.	-13.69	-7.96	1.51
eq. (8)	-12.91	-4.59	1.50
eq. (9)	-13.45	-7.74	1.51

IV. Conclusion

This paper presents an innovative antenna architecture that employs the technique of digital beam forming to improve the imaging performance and radiometric resolution of future SAR systems without loosing wide swath coverage. Long chirp signals and large reflectors, however, require more sophisticated signal processing techniques to optimize the performance. A practical solution is the use of digital finite impulse response filters with time variant coefficients in order to adapt to the chirp spectrum. By extending these space time adaptive processing concepts, also inherent modulation effects of reflector systems can be compensated. Reflectors with digital feed arrays are therefore a promising concept for future SAR systems with high potential to outperform planar arrays with regard to the SAR imaging performance for a given weight, size and cost budget.

References

[1] G. Krieger, N. Gebert, and A. Moreira, "Multidimensional Waveform Encoding: A New Digital Beamforming Technique for Synthetic Aperture Radar Remote Sensing," *IEEE Transactions on Geoscience and Remote Sensing*, vol. 46, no. 1, pp. 31–46, Jan 2008.

[2] G. Krieger, N. Gebert, M. Younis, F. Bordoni, A. Patyuchenko, and A. Moreira, "Advanced Concepts for Ultra-Wide-Swath SAR Imaging," in *European Conference on Synthetic Aperture Radar (EUSAR)*, vol. 2, Jun 2008, pp. 31–34.

[3] C. Fischer, C. Schaefer, and C. Heer, "Technology Development for the HRWS (High Resolution Wide Swath) SAR," in *International Radar Symposium (IRS)*, Sep 2007.

[4] P. T. Lam, S.-W. Lee, D. C. D. Chang, and K. Lang, "Directivity Optimization of a Reflector Antenna with Cluster Feeds: A Closed-Form Solution," *IEEE Transactions on Antennas and Propagation*, vol. 33, no. 11, pp. 1163–1174, Nov 1985.

[5] A. Patyuchenko, M. Younis, S. Huber, and G. Krieger, "Performance Optimization of the Reflector Antenna for the Digital Beam-Forming SAR System," in *Proceedings of Advanced RF Sensors and Remote Sensing Instruments (ARSI)*, 2009.